Available online at www.sciencedirect.com
ScienceDirect
Ceramics International 37 (2011) 1747–1754
CERAMICS INTERNATIONAL
www.elsevier.com/locate/ceramint

Fabrication of bulk AlN–TiN nanocomposite by reactive ball milling and underwater shock consolidation technique

H. Amini Mashhadi [a,*], N. Wada [a], R. Tomoshige [b], P. Manikandan [a], K. Hokamoto [c]

[a] Graduate School of Science and Technology, Kumamoto University, Japan
[b] Department of Nanoscience, Faculty of Engineering, Sojo University, Japan
[c] Shock Wave and Condensed Matter Research Center, Kumamoto University, Japan

Received 30 August 2010; received in revised form 19 January 2011; accepted 25 January 2011
Available online 18 February 2011

Abstract

Reactive milling of aluminum nitride and titanium powders corresponding to the stoichiometric reaction Ti + AlN resulted in the formation of the ceramic matrix composite AlN–TiN. Prolongation of the milling process led to a microstructure with nanosize range of crystallites of both AlN and TiN, evidenced through XRD measurements, SEM and TEM observation. Further, underwater shock compaction with a pressure level of about 10 GPa was applied to the nanocomposite powders to obtain bulk nanostructured sample. The effect of this shock compaction on the prolonged milled powder resulted in a 22% reduction in crystallite size. The average microhardness of the consolidated nanocomposite was 656 HV and 840 HV for 40 h and 100 h MA samples, respectively, with densities 98% of theoretical values in both cases as well as no change in chemical composition.

Keywords: B. Nanocomposites; Mechanical alloying; Underwater shock compaction; Aluminum nitride; Titanium nitride

1. Introduction

Nanocrystalline structures poses superior properties such as high strength, hardness and elastic modulus [1,2], and thus have attracted attention as high-performance materials. The process of mechanical alloying (MA) is a common method for the synthesis of ceramic matrix based nanocomposites [3]. The advantage of MA is that both matrix and reinforcement formation are an in situ process [4]. The in situ composites produced by MA possess clean, contaminant free matrix–reinforcement interfaces, which promote good bonding between matrix and reinforcement. Moreover, MA allows a homogeneous distribution of nanosized reinforcing particles in the matrix [5–8].

MA includes a process called mechanochemistry [9], in which chemical reactions and phase transformations occur due to the application of mechanical energy.

This process includes exchange reactions, reduction/oxidation reactions, compound decomposition and phase transformations.

Usually, these reactions are characterized by a large negative free energy change that can occur as a gradual transformation or as a self-propagating combustion according to milling conditions [10]. The resulting product depends on the composition of the starting powder mixture. For example, a reduction reaction of aluminum nitride by titanium can result in the ceramic matrix:

$$AlN + Ti \rightarrow TiN + Al$$

with a varying ceramic phase as a matrix together with nanocrystalline structures.

Commercial applications, however, require that these powders be compacted to obtain bulk nanocomposites, a process that demands high pressure and temperature [11]. It has been observed that the elevated temperature at conventional method require, cause excessive grain growth [4] leading to degradation of the nanocrystalline structures. Earlier work [12–18], though, has shown that this grain growth can be inhibited by very high pressure applied during consolidation.

* Corresponding author. Tel.: +81 80 4276 1706; fax: +81 96 342 3293.
E-mail addresses: amir_hie@yahoo.com, hossein1@shock.smrc.kumamoto-u.ac.jp (H.A. Mashhadi).

0272-8842/$36.00
doi:10.1016/j.ceramint.2011.01.036

Explosive compaction, an alternative method for compaction of nanocrystalline powders [22] utilizes a very rapid and intense deposition of shock energy to the powder particle surfaces to produce consolidation [19,20]. Shock waves originating from an explosive detonation can create pressure from a few to tens of GPa, resulting in inter-particle bonding in microseconds [21]. Still, explosive compaction also creates very high temperatures, which may cause melting and excessive grain growth leading to partial depletion of nanocrystalline structures [23,24]. Underwater shock compaction, an underwater shock wave generated by the detonation of an explosive for compaction [24,25], was envisioned as a technique to overcome the temperature problem. During pressurization and acceleration by the underwater shock wave, an intensive deformation of the powder surface is induced which causes the powder surfaces to undergo melting and solidification in microseconds. Material which is fully dense yet retains its nanocrystalline structure is possible due to the absence of overheating and the associated excessive grain growth. Hence, the aim of the present work is to produce "in situ" nanocrystalline AlN–TiN ceramic matrix nanocomposite powders through reactive milling and to consolidate the same using underwater shock compaction technique.

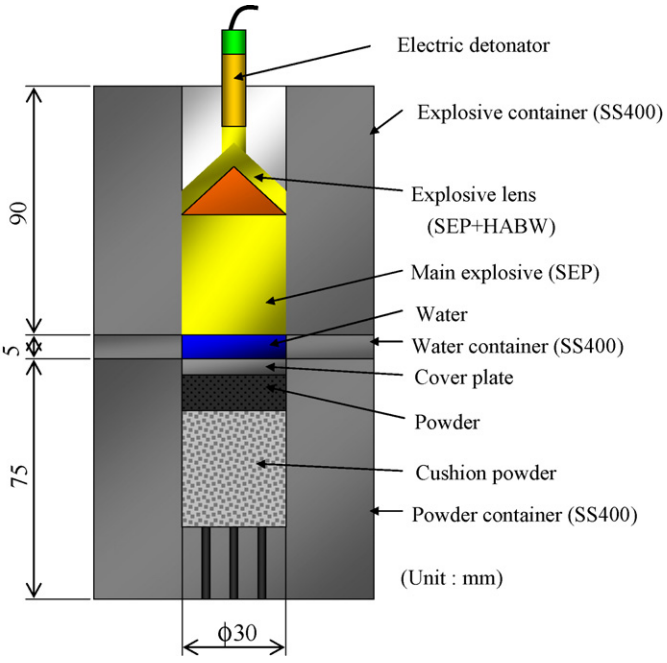

Fig. 1. Schematic illustration of underwater shock compaction apparatus.

2. Experimental procedure

2.1. Milling details

Mixtures of aluminum nitride and titanium powders with a molar ratio of 1:1 were prepared, from starting powders of Ti (99.7% pure, max. particle size 45 μm), and agglomerated AlN powder. A Fritsch Pulverisette P6 planetary ball mill was used for the reactive ball milling processes under the milling conditions given in Table 1. Milling was interrupted at regular intervals for characterization. Powder handling was performed in a glove bag under an argon atmosphere.

2.2. Assembly design of shock compaction apparatus

The underwater shock compaction apparatus, which it's schematic is shown in Fig. 1, was composed of five parts: explosive lens, explosive container, water container, powder container and cover plate. Two types of explosives: SEP and HABW (both supplied by Asahi-Kasei Chemicals Corp., Japan); detonation velocity: 6.97 and 4.75 km/s, respectively; density: 1300 and 2200 kg/m^3, respectively, were used in the explosive lens to create planar waves. The explosive SEP (PETN 65% mass and paraffin 35% mass) was set in the explosive container as the main explosive. The water container, made of mild steel with dimensions of 5 mm height and 70 mm diameter was filled with water for the underwater shock wave to propagate through it. Shock pressure magnitude was controllable by adjusting the height of the water container. The magnitude of shock pressure used in this work was estimated as 10 GPa based on numerical simulation [26], almost identical to the actual pressure magnitude as measured using a Manganin gauge developed by Mashimo and a co-worker [27]. The milled powder was filled and pressed into the powder container using a uniaxial press machine at a pressure of 50 MPa. The powder container, made of mild steel, had an inner diameter of 30 mm, a height of 75 mm, a powder charging depth of 50 mm, and a gas drain hole of 2 mm diameter to allow trapped air to escape during compaction. The thickness of the pressed powder was approximately 10 mm. The cover plate was made of stainless steel with a thickness of 2 mm and was placed on top of the powder.

Table 1
Milling conditions.

Mill	Planetary ball mill
Milling speed (rpm)	250
Ball to powder ratio "BPR"	10:1
Diameter of milling ball (mm)	10
Process control agent "PCA"	1% stearic acid
Volume of milling vial (ml)	500
Weight of each milling ball (g)	4
Milling time (h)	2.5, 5, 10, 20, 40, 100

2.3. Sample characterization

Observations and characterizations of the powders and the consolidated composite were carried out using optical microscope (OM), SEM, TEM, EPMA and X-ray diffraction (XRD). The XRD investigations were performed using a Rigaku Denki ultra X 18VB2-3 with Cu Kα radiation (λ = 0.15418 nm). Scanning electron microscopy (SEM) observations of the powder particles size and morphology were performed using a JEOL (JCM-5700) at an accelerating voltage of 15 kV. Structural observations of the powders by transmission electron microscopy (TEM) were carried out with

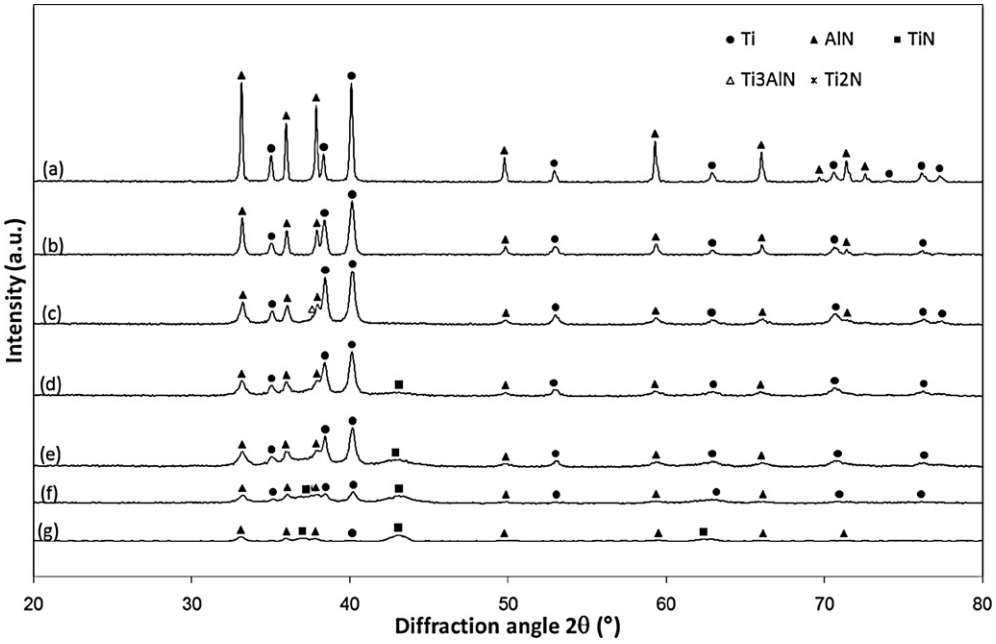

Fig. 2. XRD patterns of Ti + AlN mixture milled for different times: (a) mixed powder; (b) 2.5 h; (c) 5 h; (d) 10 h; (e) 20 h; (f) 40 h; (g) 100 h [28].

a Philips TECNAI F20 microscope. The microhardness of the compacts was measured using a HM-221 microhardness tester under a load of 100 g imposed for 10 s. Each reported value represents an average of three indents. Determination of chemical composition was done by electron probe micro analyzer (EPMA) point scan using an EPMA, Model 1720/1720H, Japan SHIMADZU. Finally, density of the shock compacted samples was measured using a LIBROR AEL-200 balance equipped with a device for measuring the density of solids (Archimedes method).

3. Results and discussion

Fig. 2 shows the XRD patterns of powders collected over increased milling times, based on the previous work of the authors [28]. For milling time of up to 10 h, no phase transformation was observed. However, the broadening of the diffraction lines of Ti and AlN is considerable, testifying to the decrease of crystallite size and increase of lattice strain. The reduction reaction of AlN under the effect of Ti takes place after 5 h of MA. This is evident from the XRD pattern of powders collected after 5 h consisting of the diffraction lines of TiN which formed in situ directly during the ball milling process. The XRD patterns also show that a considerable portion of AlN particles remained after 100 h MA. This is related to the partial reaction between Ti and AlN during the mechanical alloying (MA) due to low adiabatic temperature and milling intensity insufficient to activate the exchange reaction ($AlN + Ti \rightarrow TiN + Al$). Thermodynamical calculation of this reaction showed that it was unable to progress via mechanically induced self-propagation reaction (MSR) and underwent gradual mode. This means that the accumulated energy of milled powder after 100 h MA is insufficient to complete the transformation. Also, because there was no other nitrogen provider except AlN during MA, Ti merely seizes nitrogen atoms from AlN particles to form in situ TiN. Beside this, the covalent nature of AlN and strong affinity of Al to N cause low diffusion rate. However, as MA is a non-equilibrium

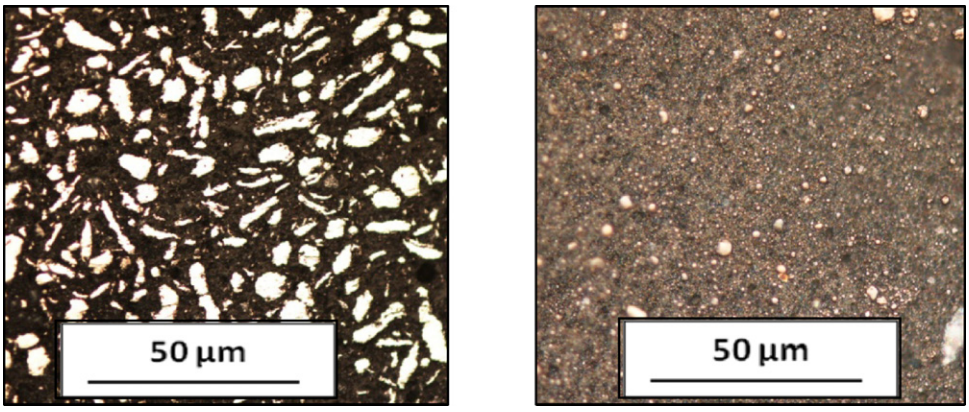

Fig. 3. Optical images of the cross-section of the milled samples, (a) after 2.5 h MA, (b) after 100 h MA.

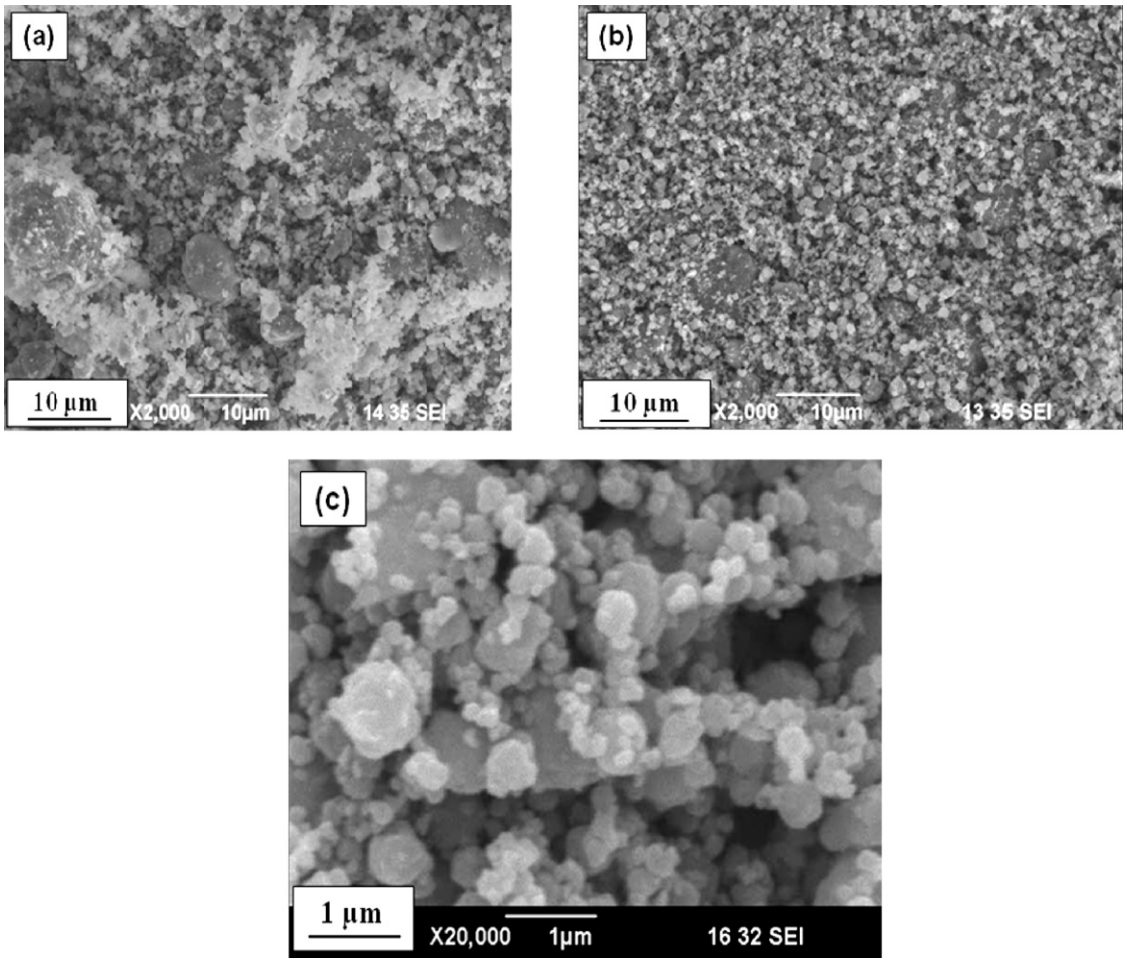

Fig. 4. Morphologies of the milled powders for (a) 20 h, (b) 40 h and (c) 100 h (different magnification).

process, a metastable over saturated solid solution of Al and N in Ti can be obtained at high concentration well above those predicted by thermodynamics. It has been published by the authors [28] that the entire Al resulted from decomposed AlN particles was completely dissolved in Ti lattice, according to the maximum solubility of Al in Ti lattice by MA. An average crystallite size of less than 15 nm was obtained for TiN particles according to estimation by the Scherrer formula.

Fig. 3 shows optical images of the cross section of the powders milled for 2.5 and for 100 h. Increasingly fine particle size with prolonged ball milling is apparent. AlN particles (white particles) are believed to act as a milling agent and hasten refining [29]. Fig. 4 shows SEM micrographs of milled samples at three different MA time intervals: 20, 40 and 100 h. The completely equiaxed morphology of particles after 40 h of MA is clearly visible, which is the characteristic of particles at steady state. A very fine particle size can also be seen after 100 h of MA with the average particle size of about 300 nm (Fig. 4c).

The initial structure of the powder mixture determines the energy flow and distribution in the sample during shock loading. Therefore, the samples after 40 and 100 h of MA, which have the finest and most equiaxed morphology, were subjected to shock compaction. Fig. 5 shows SEM cross-section images of the MA powder particles and subsequent shock compacted samples. Comparison of pre- and post-shock compaction images in Fig. 5a–d, representing 40 h and 100 h of MA, reveals a dramatically different microstructure. This difference is attributed to extensive plastic deformation and solid-state interfacial bonding induced due to the passage of the shock wave through the water medium and into the milled powders, confirming that the powders were deformed significantly to fill the voids, though a few pores exist at the grain boundaries. It is noticeable that the porosity may be due to the larger initial size of the particles which, when precompacted, leave intermedial empty air. When the shock wave passes throughout this region, this empty space forms porosity in the consolidated specimens (Fig. 6a). Measured values of the relative density shows that about 98% of theoretical density was achieved for both 40 h and 100 h MA shock compacted samples (3.79 g/cm^3 versus 3.83 g/cm^3 of theoretical density).

It is worth noting that, during shock consolidation processing, cracks are easily generated by high shock energy, reflected tensile waves and residual stresses generated by rapid cooling of the compacts after shock loading [23], as can be seen in Fig. 6b.

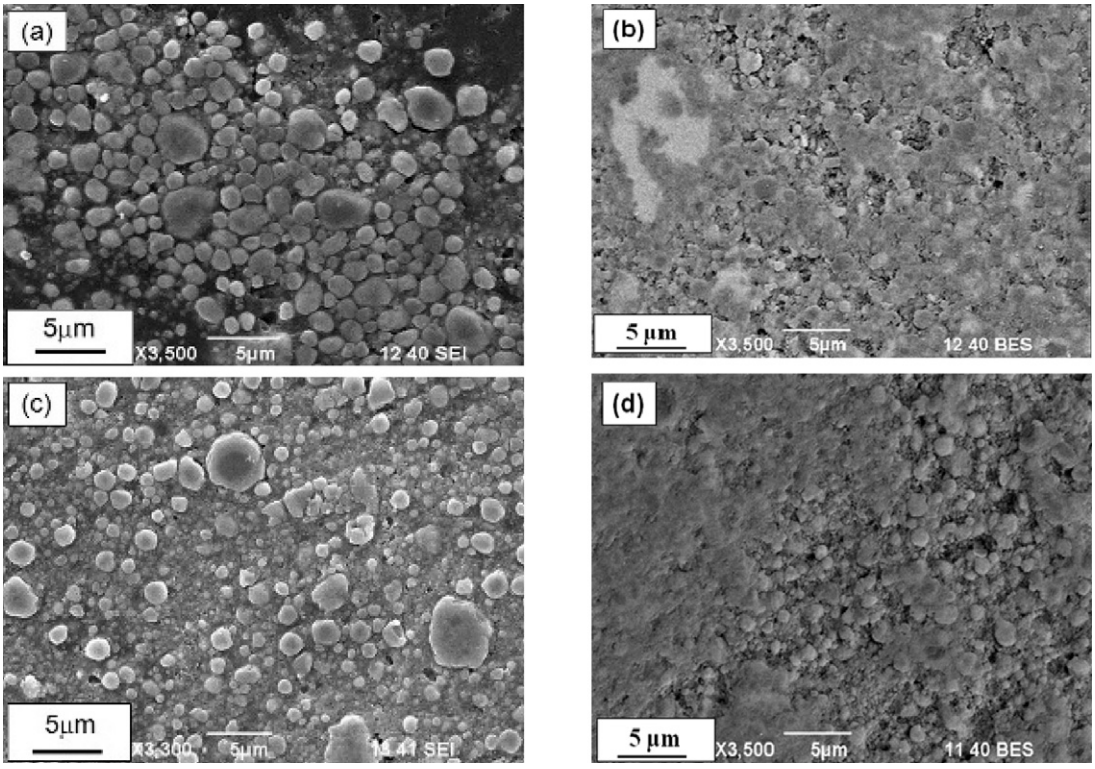

Fig. 5. SEM images of cross-sections of the milled powder (a, c) and shock compacted samples (b, c) for 40 h and 100 h MA, respectively.

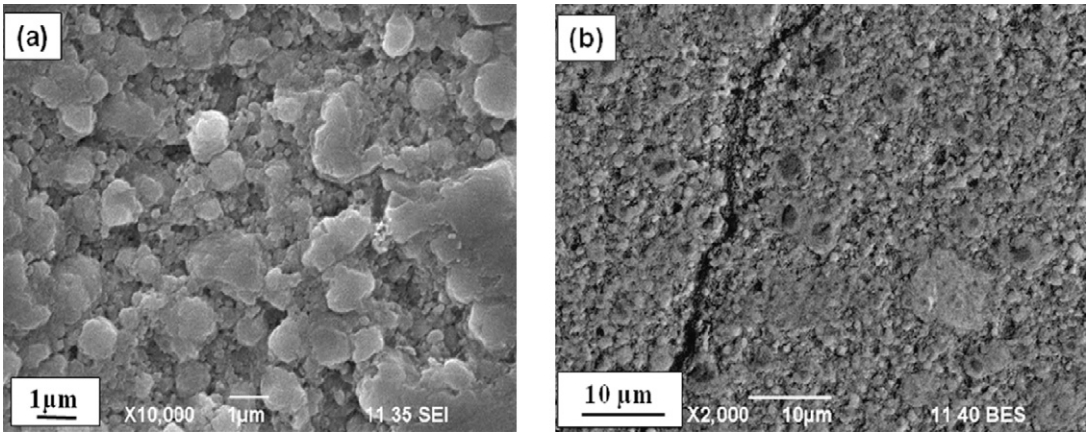

Fig. 6. SEM image cross-sections of shock compacted of 100 h MA sample showing: (a) the presence of porosity and (b) microcrack.

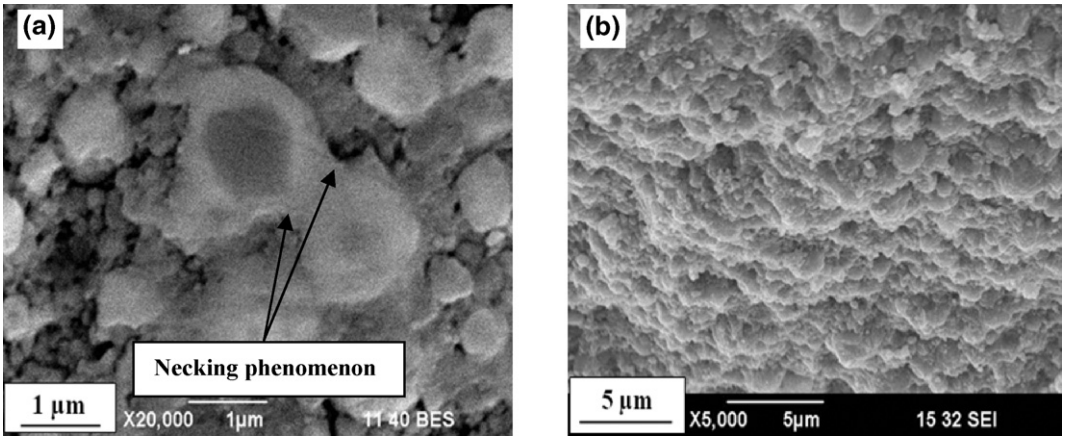

Fig. 7. SEM images of the shock compacted of 100 h MA time; (a) neck growth between two particles following shock compaction, (b) fracture surface.

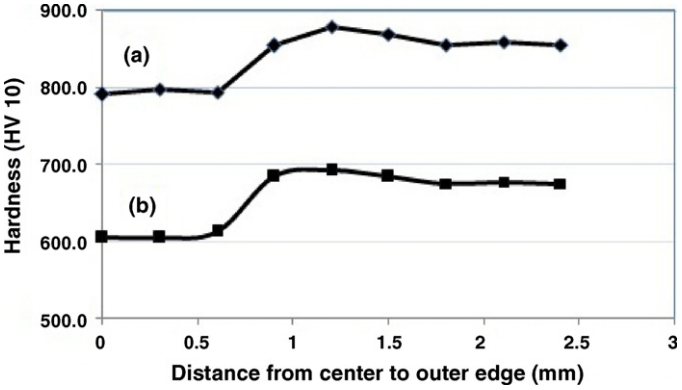

Fig. 8. Microhardness across the cross-section of shock compacted samples from the center to the outer edge of (a) after 100 h MA and (b) after 40 h MA.

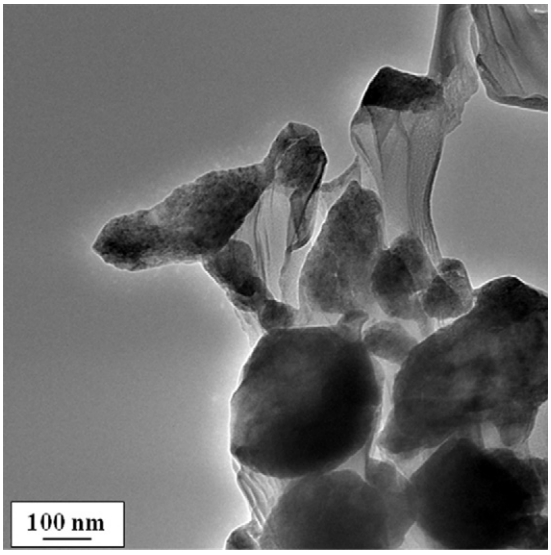

Fig. 9. TEM image of a 100 h MA sample.

The sample developed after shock compaction has a uniform and fine-grained composite structure. The powders after shock loading appear to have slightly enlarged, possibly caused by the conjunction of original powders through surface melting. It is believed that the shock compaction leads to localized deformation and melting of the particle surfaces, as illustrated in Fig. 7. Fig. 7a shows a typical neck growth between two round grains following exposure to shock compaction, with full contact between the grains, magnified from the fracture surface of shock consolidated sample after 100 h of MA shown in Fig. 7b. This result fully agrees with other research [30–32]. The measured densities and microstructures as seen in Figs. 6 and 7 illustrate how the shock waves impact the MA powders, leading to successful bonding with strong cohesion between the powders as well as a noticeable elimination of voids.

Fig. 8 shows variation of microhardness across the cross-section of the consolidated samples, with each point displaying the average of three measurements. The data shows only a slight variation of hardness across the cross-section of consolidates, indicating almost uniform densification. The trend to increasing hardness towards the consolidate edge is probably due to the presence of more voids in the consolidate center as compared to the periphery, as revealed in Fig. 8, attributable to the higher temperatures being generated towards the center of the shocked specimens. Similar results were obtained by Marquis et al. on shock consolidation of tungsten-based heavy alloys [33]. Microhardness varying according to MA time for 40 h and 100 h is also apparent in Fig. 8. A significantly higher hardness of shock compacted sample of 100 h MA over that of 40 h MA is notable. This variation of hardness is believed to be caused by two factors: the high-energy milling process, which introduces more work hardening and severe deformation into powder [34]; and the greater formation of in situ TiN particles over increased milling time, particles which are relatively hard (2300 HV) [35], as well as the greater refinement of AlN particles with increased milling time.

In order to evaluate the effect of shock compaction on chemical composition of MA sample, quantitative analysis by EPMA point scan in selected area of milled and consolidated samples was performed (Table 2). Notably, in the present work, MA powder was maintained under an argon atmosphere whenever possible. However, oxygen contamination is unavoidable, for example, when packing the powder into recovery-fixture capsules in addition to possible contamination of initial powders. Besides, the existence of a significant amount of carbon and oxygen is related to the addition of stearic acid ($C_{18}H_{36}O_2$) as a process control agent (PCA) in order to avoid excessive cold welding that would lead to an increase in particle size and considerable sticking of the powders to the milling tools [3]. The presence of oxygen could also be related to the trace amounts of oxygen in the argon filled glove box used for powder handling. However, it can be seen that there is no considerable change of composition before and after explosive compaction in major elements like Ti, Al and N. The negligible change in the amount of C suggests that there is no contamination of this element during shock processing. The existence of other elements such as Fe, Ni and Cr are related to the contamination of powder with milling tools during prolonged MA time.

Fig. 9 is a TEM micrograph of 100 h MA powder showing agglomerated crystalline nanoparticles. Such agglomeration of

Table 2
EPMA point scan results of detected chemical compositions (wt%) before and after shock compaction.

Process	Ti	Al	N	Fe	Ni	Cr	C	O	Au[a]
After 100 h MA	44.26	20.32	20.30	1.84	0.19	0.57	1.78	3.75	6.58
After shock consolidation	43.48	21.60	19.01	1.96	0.2	0.53	1.75	4.45	7.02

[a] The presence of Au is due to the use of gold coating in EPMA study of samples.

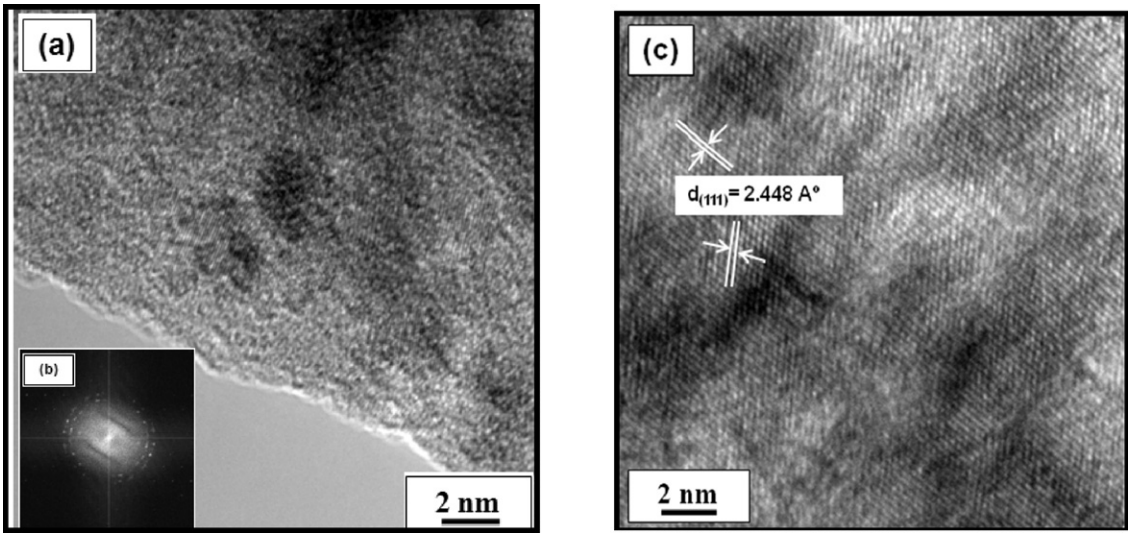

Fig. 10. TEM micrographs of 100 h milled powder (a) HR-TEM image together with associated SADP (b), (c) HR-TEM represent crystalline wall of TiN phase.

nanoparticles is usually attributable to minimization of surface free energy. Fig. 10a and b presents a bright field TEM image and selected area diffraction pattern (SADP) of milled powder. The crystallites observed are ∼15 nm, consistent with XRD analysis using the Scherrer method. The fine grains align as spots in a ring-shaped SADP (Fig. 10b) and clearly demonstrate that the particles are nanocrystalline. The diffusive rings of the selected area diffraction pattern suggest an amorphous structure. Many research works have notably indicated that MA of a range of different materials leads to the formation of some amorphous structures [36,37]. High resolution TEM observation confirms the nanocrystalline nature of the composite and the presence of in situ TiN after prolonged MA as well. The HR-TEM image of 100 h MA powder (Fig. 10c) reveals crystalline walls with reticular distance of 2.448 Å corresponding to the (1 1 1) face spacing of TiN phase.

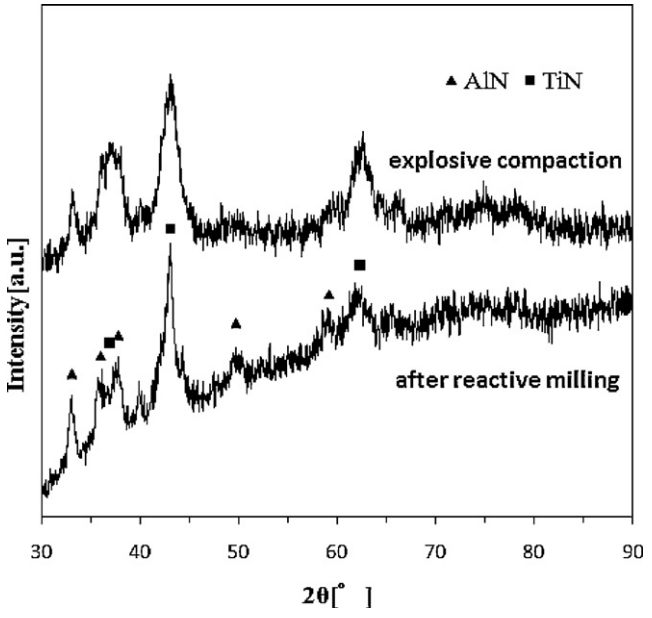

Fig. 11. XRD patterns of the samples after 100 h of MA and under water shock compaction.

XRD patterns of samples after 100 h MA and explosive compaction are presented in Fig. 11. The sole difference between the two traces is the increased width of diffraction peaks in the explosively compacted sample, indicating a slight of the grain size during shock compaction, which is in agreement with earlier results [30,31,38]. The crystallite size of the main peak of TiN(2 0 0) appears as 12.2 nm for the shock consolidated sample as opposed to 15.7 nm for the sample after 100 h MA. The retention of ultra-fine grain size is likely due to minimization of otherwise detrimental effects of heating associated with the dynamic compaction process and also from the controlled aspect of the powder shock wave consolidation. There are also no significant differences between the patterns, with the similarity of the two results confirming there is no phase transformation by shock compaction.

4. Conclusions

A synthesis method for producing bulk nanocomposite using mechanosynthesis followed by underwater shock compaction was investigated.

Reactive ball milling of Ti and AlN resulted in the formation of a nanostructural AlN–TiN composite. Precursor AlN–TiN powders were successfully densified using underwater shock compaction without sintering aids. Shock-compacted samples showed high density and microhardness. Increased hardness in proportion to milling time in the average of 656–840 $HV_{0.1}$ was observed due to the formation of solid solution as well as work hardening and further refinement of the components.

The high density of the compacts obtained is attributed to the strong solid-state bonding and retention of fine morphology through the shock compression. The nanoscale grain size was retained after the consolidation process and bulk nanocrystalline AlN–TiN composite with a mean 12 nm crystallite size of in situ TiN phase was obtained. Quantitative analysis showed

that using underwater shock compaction has no considerable effect on chemical composition or contamination of the nanocomposite. The result, together with those of structural investigation ascertains that the present method of MA and dynamic compaction preserves nanocrystalline structure of the composite and improves quality of compaction with the exception of, minor surface micro-cracks.

Acknowledgements

This work was supported by Global COE program. The authors also would like to thank L. Chen, G. Kennedy and W. Baerg for their kind cooperation and expert comments.

References

[1] G.W. Nieman, J.R. Weertman, R.W. Siegel, Mechanical behavior of nanocrystalline metals, Nanostruct. Mater. 1 (1992) 185–190.
[2] R.W. Siegel, G.E. Fougere, Mechanical properties of nanophase metals, Nanostruct. Mater. 6 (1995) 205–216.
[3] C. Suryanarayana, Mechanical alloying and milling, Prog. Mater. Sci. 46 (2001) 1–184.
[4] M. Krasnowski, T. Kulit, Nanocrystalline FeAl–TiN composites obtained by hot-pressing consolidation of reactively milled powders, Scr. Mater. 57 (2007) 553–556.
[5] C.C. Koch, Intermetallic matrix composites prepared by mechanical alloying—a review, Mater. Sci. Eng. A 244 (1998) 39–48.
[6] M. Krasnowski, T. Kulik, Nanocomposites obtained by mechanical alloying in Fe–Al–Ti–C system, J. Alloys Compd. 448 (2008) 227–233.
[7] M. Krasnowski, H. Matyja, Structural investigations of the TiC–Fe(Al) nanocomposite formed by mechanical alloying, Mater. Sci. Forum 343–346 (2000) 302–307.
[8] M. Krasnowski, H. Matyja, Synthesis of FeAl–TiN nanocomposite by mechanical alloying of Al–Fe–Ti powder mixture under nitrogen atmosphere, Mater. Sci. Forum 360–362 (2001) 433–438.
[9] L. Takacs, Self-sustaining reactions induced by ball milling, Prog. Mater. Sci. 47 (2002) 355–414.
[10] D. Oleszak, NiAl–Al_2O_3 intermetallic matrix composite prepared by reactive milling and consolidation of powders, J. Mater. Sci. 39 (2004) 5169–5174.
[11] M. Rosso, Ceramic and metal matrix composites: routes and properties, J. Mater. Process. Technol. 175 (2006) 364–375.
[12] R. Chaim, Densification mechanisms in spark plasma sintering of nanocrystalline ceramics, Mater. Sci. Eng. A 443 (2007) 25–32.
[13] J. Rawers, Comparison of attrition milled, nanostructured, powder-compaction techniques, Nanostruct. Mater. 11 (1999) 513–522.
[14] M.J. Mayo, Processing of nanocrystalline ceramics from ultrafine particles, Int. Mater. Rev. 41 (1996) 85–115.
[15] M. Krasnowski, T. Kulik, Nanocrystalline FeAl intermetallic produced by mechanical alloying followed by hot-pressing consolidation, Intermetallics 15 (2007) 201–205.
[16] H.H. Hng, L. Halim, Grain growth in sintered ZnO–1 mol% V_2O_5 ceramics, Mater. Lett. 57 (2003) 1411–1416.
[17] R.R. Menezes, R.H.G.A. Kimimami, Microwave sintering of alumina–zirconia nanocomposites, J. Mater. Process. Technol. 203 (2008) 513–517.
[18] M. Mazaheri, A.M. Zahedi, S.K. Sadrnezhaad, Two-step sintering of nanocrystalline ZnO compacts: effect of temperature on densification and grain growth, J. Am. Ceram. Soc. 91 (2008) 56–63.
[19] P. Manikandan, A.N. Faruqui, K. Raghukandan, A. Mori, K. Hokamoto, Underwater shock consolidation of Mg–SiC composites, J. Mater. Sci. 45 (2010) 4518–4562.
[20] Y. Kim, H. Wada, Y. Lee, S. Itoh, Magnetization, Magnetic transition and magnetic entropy changes of bulk $MnAs_{1-x}Sb_x$ fabricated by underwater shock compaction, Mater. Sci. Eng. B 167 (2010) 114–118.
[21] Z.-Q. Jin, C. Rockett, J. Ping Liu, K. Hokamoto, N.N. Thadhani, Underwater explosive shock consolidation of nanocomposite Pr 2Fe14B/α-Fe magnetic powders, Mater. Trans. 2 (2005) 372–375.
[22] N.N. Thadhani, Dynamic shock compaction of nanocrystalline bulk magnetic and thermoelectric materials, Mater. Sci. Forum 426–432 (2003) 2357–2362.
[23] K. Hokamoto, S. Tananka, M. Fujita, S. Itoh, M.A. Meyers, H.C. Chen, High temperature shock consolidation of hard ceramic powders, Physica B 239 (1997) 1–5.
[24] A. Chiba, S. Kimura, K. Raghukandan, Y. Morizono, Effect of alumina addition on hydroxyapatite biocomposites fabricated by underwater-shock compaction, Mater. Sci. Eng. A 350 (2003) 179–183.
[25] Z.Q. Jin, K.H. Chen, J. Li, H. Zeng, S.F. Cheng, J.P. Liu, Z.L. Wang, N.N. Thadhani, Shock compression response of magnetic nanocomposite powders, Acta Mater. 52 (2004) 2147–2154.
[26] K. Hokamoto, J.S. Lee, M. Fujita, S. Itoh, K. Raghukandan, The synthesis of bulk material through explosive compaction for making intermetallic compound Ti5Si3 and its composites, J. Mater. Sci. 37 (2002) 4073–4078.
[27] A. Nakamura, T. Mashimo, Calibration experiments of a thin manganin gauge for shock-wave measurement in solids: measurements of shock-stress history in alumina, J. Appl. Phys. 32 (1993) 4785–4790.
[28] H. Amini Mashhadi, P. Manikandan, R. Suetsugu, S. Tanaka, K. Hokamoto, Synthesis of AlN–TiN nanostructured composite powder by reactive ball milling and subsequent thermal treatment, J. Alloys Compd. 506 (2010) 653–660.
[29] Z. Razavi Hesabi, A. Simchi, S.M. Seyed Reihani, Structural evolution during mechanical milling of nanometric and micrometric Al_2O_3 reinforced Al matrix composites, Mater. Sci. Eng. A 428 (2006) 159–168.
[30] K. Hokamoto, R.A. Pruemmer, R. Kniter, K. Taira, Hot explosive compaction of diamond powder using cylindrical geometry, J. Mater. Sci. 43 (2008) 684–688.
[31] Y. Kim, T. Ueda, K. Hokamoto, S. Itoh, Electric and microstructural characteristics of bulk ZnO fabricated by underwater shock compaction, Ceram. Int. 35 (2009) 3247–3252.
[32] K. Raghukandan, K. Hokamoto, J.S. Lee, A. Chiba, B.C. Pai, An investigation on underwater shock consolidated carbon fiber reinforced Al composites, J. Mater. Process. Technol. 134 (2003) 329–337.
[33] F.D.S. Marquis, A. Mahsjan, A.G. Mamalis, Shock synthesis and densification of tungsten based heavy alloys, J. Mater. Process. Technol. 161 (2005) 113–120.
[34] Z. Razavi Hesabi, H.R. Hafizpour, A. Simchi, An investigation on the compressibility of aluminum/nano-alumina composite powder prepared by blending and mechanical milling, Mater. Sci. Eng. A 454 (2007) 89–98.
[35] J. Ding, T. Tsuzuki, P.G. McCormick, Ultrafine alumina particles prepared by mechanochemical/thermal processing, J. Am. Ceram. Soc. 79 (1996) 2956–2958.
[36] M. Bodaghi, A. Mirhabibi, M. Tahriri, H. Zolfonun, M. Karimi, Mechanochemical assisted synthesis and powder characteristics of nanostructure ceramic of α-Al_2O_3 at room temperature, Mater. Sci. Eng. B 162 (2009) 155–161.
[37] W.L.E. Wong, S. Karthik, M. Gupa, Development of high performance Mg–Al_2O_3 composites containing Al_2O_3 in submicron length scale using microwave assisted rapid sintering, Mater. Sci. Technol. 31 (2005) 1063–1070.
[38] Z.Q. Jin, C. Rockett, J. Ping Liu, K. Hokamoto, N.N. Thadhani, Underwater explosive shock consolidation of nanocomposite Pr 2Fe14B/α-Fe magnetic powders, Mater Trans. 46 (2005) 372–375.